Three-dimensional simulations of quantum transport in semiconductor nanostructures

D. Z.-Y. Ting, S. K. Kirby, and T. C. McGill
Thomas J. Watson, Sr., Laboratory of Applied Physics, California Institute of Technology, Pasadena, California 91125

(Received 3 February 1993; accepted 24 March 1993)

We introduce the planar supercell method as a means for treating three-dimensional quantum transport in mesoscopic tunnel structures. Our model treats potential variations along the growth direction as well as the lateral directions. The flexibility of the method allows us to examine a variety of physical phenomena relevant to quantum transport, including alloy disorder, interface roughness, defect impurities, and zero-dimensional, one-dimensional, and two-dimensional quantum confinement, in a variety of device geometries ranging from double barrier heterostructures to quantum wire electron waveguides. Using this method, we have studied the transport properties of double barrier heterostructures with alloy barriers, including the effect of clustering in the alloy layers. We have also examined interface roughness in double barrier structures, and analyzed $\mathbf{k}_\parallel$ scattering and lateral localization. In addition, we have studied the transport properties of a quantum wire electron waveguide, and explored its sensitivity to the geometry of waveguide openings.

I. INTRODUCTION

In modeling quantum transport in semiconductor resonant tunneling heterostructures, one can often assume perfect periodicity in the lateral directions, and thereby reducing the mathematical description to a one-dimensional (1D) problem in which only the potential variation along the growth direction need be considered. However, in realistic device structures we need to take into account imperfections such as interface roughness, impurities, and alloy disorder which are incompatible with the assumption of translational invariance in the parallel directions. In this work, we introduce the planar supercell method as a general purpose model for treating these structural imperfections. The model is designed for flexibility so that it can be used not only to study tunnel structures such as the double barrier heterostructure, but also novel mesoscopic devices such as quantum wire electron waveguides. Using this method, we have studied how the transport properties of double barrier heterostructures are influenced by alloy disorder (including clustering effects), and interface roughness. We also briefly report on a study of transport in quantum wire electron waveguides.

II. METHODS

We have employed a planar supercell tight-binding Hamiltonian in our treatment of nanostructures with three-dimensional (3D) features. A structure is specified as a collection of N_z layers perpendicular to the z direction, with each layer containing a periodic array of rectangular planar supercells of $N_x \times N_y$ sites. Within each planar supercell, the potential can take on lateral variations as dictated by the device geometry. Although several orbitals can be placed at each site, our current model uses one s-like orbital per unit cell. On-site and nearest-neighbor matrix elements are chosen to yield the correct local potential and effective mass values. Our model is thus formally equivalent to the one-band effective mass equation[1]

$$-\frac{\hbar^2}{2}\nabla\cdot\frac{1}{m(x)}\nabla\psi+V(x)\psi=E\psi, \tag{1}$$

discretized over a Cartesian grid, and subject to periodic boundary conditions (with supercell periodicity) in the x and y directions, and open boundary conditions in the z direction.

The transmission coefficients for structures described by the planar supercell stack can be determined by the direct application of the 1D multiband method described by Ting *et al.*,[2] since the single-band planar supercell model may be considered as a 1D multiband model with $N_x \times N_y$ bands. In this method, calculating each transmission coefficient requires the solution of a sparse system of $2N_xN_yN_z$ coupled linear equations. Since a typical problem may involve 50 layers of 20×20 planar supercells, obtaining a single transmission coefficient requires the solution of 40 000 coupled linear equations. The accurate and efficient solutions of the large sparse linear systems is achieved with the application of the quasiminimal residual method.[3]

Unlike 1D quantum transport methods where the in-plane crystal momentum ($\mathbf{k}_\parallel$) is conserved, the planar supercell method is capable of treating $\mathbf{k}_\parallel$ scattering. In general, a given $\mathbf{k}_\parallel$ can scatter into a continuous range of $\mathbf{k}'_\parallel$. However, in the planar supercell method, due to the finite supercell size ($N_x \times N_y$ sites), $\mathbf{k}_\parallel$ can scatter only into a set of $N_x \times N_y$ parallel $\mathbf{k}$ vectors given by

$$\mathbf{k}'_\parallel = \mathbf{k}_\parallel + \mathbf{g}_{lm}, \tag{2}$$

$$\mathbf{g}_{lm}=\left(\frac{2\pi l}{N_x d_x}, \frac{2\pi m}{N_y d_y}, 0\right), \quad l=1, \ldots, N_x, \quad m=1, \ldots, N_y, \tag{3}$$

 0734-211X/93/11(4)/1738/5/$1.00

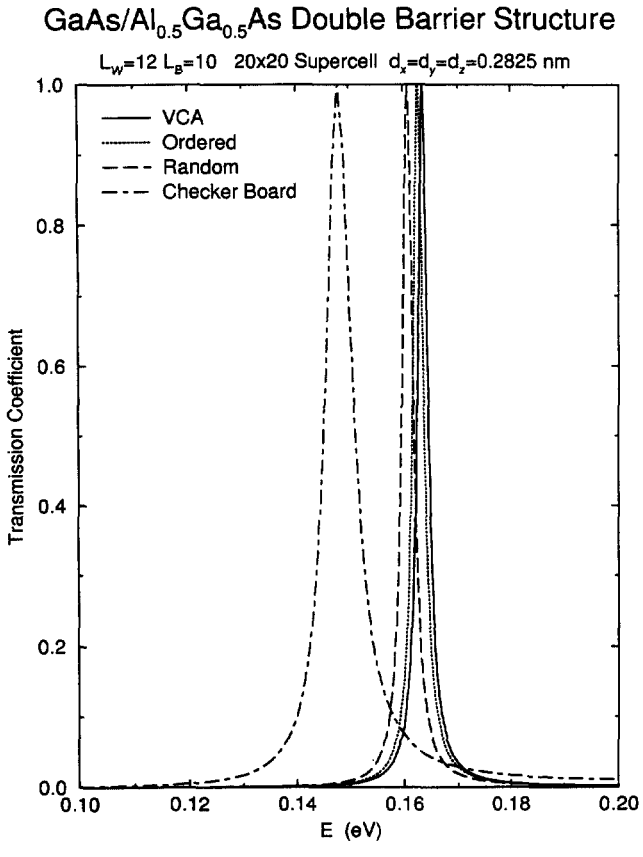

FIG. 1. Transmission coefficients for a set of double barrier structures with GaAs wells, and barriers consisting of equal amounts of AlAs and GaAs, mixed in ordered, random, and checkerboard configurations. Result for a structure with VCA $Al_{0.5}Ga_{0.5}As$ alloy barriers is also shown. The well and barrier widths are $L_W=12$ (monolayer) and $L_B=10$. Discretization sizes of $d_x=d_y=d_z=2.825$ Å are used with 20×20 planar supercells in the simulation.

where $\mathbf{g}_{lm}$'s are the $N_x\times N_y$ parallel reciprocal lattice vectors associated with the mini-Brillouin zone of the planar supercell, and d_x, d_y, and d_z are the discretization step sizes.

III. RESULTS AND DISCUSSION

We apply the planar supercell method to three examples: (1) alloy disorder in double barrier resonant tunneling structures with alloy barriers, (2) interface roughness in double barrier structures, and, (3) electron waveguides.

First, we examine transport in a (001) double barrier structure with a 12 monolayer GaAs well and 10 monolayer $Al_{0.5}Ga_{0.5}As$ barriers. The alloy barriers are simulated with 20×20 supercells consisting of random mixtures of GaAs and AlAs sites. Discretization sizes of $d_x=d_y=d_z=2.825$ Å are chosen to match the distance between adjacent monolayers along the growth direction. The material parameters for GaAs and AlAs used are: $E_C^{\mathrm{GaAs}}=0$ eV, $m^*_{\mathrm{GaAs}}=0.0673\ m_0$, $E_C^{\mathrm{AlAs}}=1.05$ eV, $m^*_{\mathrm{AlAs}}=0.1248\ m_0$. The calculated transmission coefficients for this structure is shown in Fig. 1. For comparison, we have included the results of a virtual crystal approximation (VCA) calculation, where the fluctuating random alloy potential is replaced by a smooth, averaged potential. In our example, VCA treats $Al_{0.5}Ga_{0.5}As$ as a fictitious material having the averaged properties of GaAs and AlAs. Specifically, VCA material parameters for $Al_xGa_{1-x}As$ are given by $E_C^{\mathrm{VCA}}=xE_C^{\mathrm{AlAs}}+(1-x)E_C^{\mathrm{GaAs}}$, and $1/m^*_{\mathrm{VCA}}=x/m^*_{\mathrm{AlAs}}+(1-x)/m^*_{\mathrm{GaAs}}$.

Comparing the two calculations, we note that the VCA result is in very good agreement with the supercell calculation for the random alloy configuration; the resonance peak positions differ by only 2.8 meV, and the widths are almost identical. Therefore, for practical purposes, the VCA treatment of the alloy barriers is quite satisfactory. The good agreement is not altogether unexpected; the electron de Broglie wavelength in this energy range is considerably larger than the length scale over which the random potential varies, and therefore the random potential is seen only in an averaged sense.

We can use the supercell method to examine the effect of ordering in the barrier layers. In Fig. 1 we include the results for two additional structures. In the ordered structure, the alloy layers are constructed so that each GaAs site is completely surrounded by AlAs sites, and vice versa. In the checkerboard structure, each 20×20 planar supercell in the barrier is divided into two 10×10 GaAs squares and two 10×10 AlAs squares, arranged in a checkerboard pattern. A convenient way to characterize the different types of barriers is to use the short-range order parameter ρ, defined as the ratio of the number of bonds connecting different types of sites (i.e., GaAs–AlAs), and the total number of bonds. The ordered, random, and checkerboard barriers have $\rho=1$, 0.5, and 0.07, respectively. Figure 1 shows that the transmission spectrum for the ordered structure is in even better agreement with the VCA calculation, differing only by 0.8 meV in resonance peak position. The resonance for the checkerboard structure, on the other hand, is considerably down shifted and broadened compared to the others. This is because the length scale of the potential variation in the lateral direction is significant compared to the de Broglie wavelength.

The results shown in Fig. 1 suggest that the transmission properties of double barrier structures with alloy barriers are strongly influenced by clustering in the alloy barriers. To study the effect of clustering more systematically, in Fig. 2 we show the transmission coefficients for a set of double barriers structures with varying degrees of clustering in the alloy layers. Random alloy configurations with different cluster sizes are generated with a simulated annealing algorithm.[4] An island size for each monolayer of the barrier material is calculated; the average island size is used to characterize the degree of clustering. We use a discretization size of $d_z=2.825$ Å for the z direction as before, but larger sizes of $d_x=d_y=10$ Å for the lateral directions are used so that we can simulate larger clusters and still use 20×20 planar supercells; calculations using supercells with more sites would have been more computationally demanding. Comparing the results for structures with average island sizes of 39, 69, and 102 Å and the VCA result in Fig. 2, we observe that as the cluster size increases, the resonance peak down shifts and broadens. This

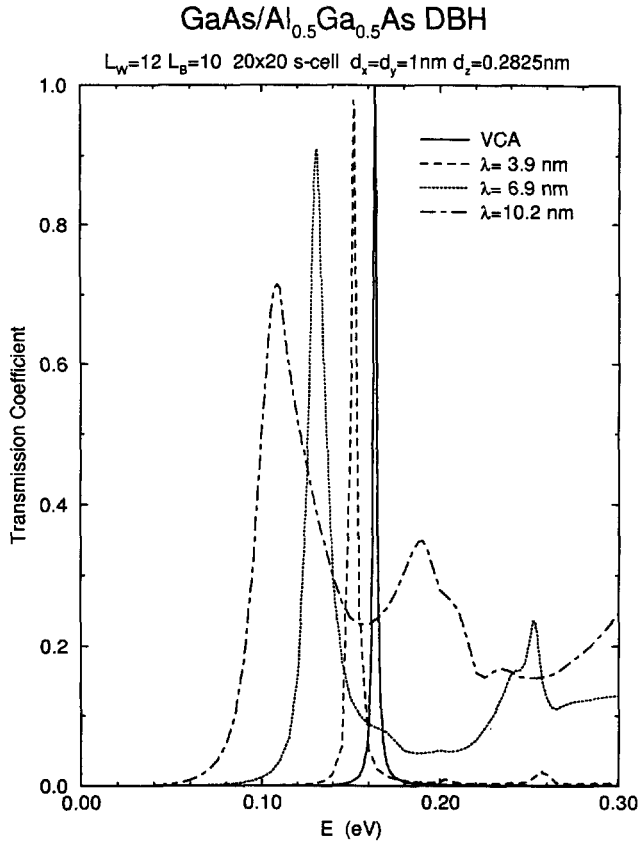

FIG. 2. Transmission coefficients for a set of double barrier structures with $L_W=12$ GaAs wells and $L_B=10$ $Al_{0.5}Ga_{0.5}As$ alloy barriers. Results for structures with varying degrees of clustering in the alloy layers (average island sizes of $\lambda=39$, 69, and 102 Å) are compared with a VCA calculation. Discretization sizes of $d_x=d_y=10$ Å and $d_z=2.825$ Å are used with 20×20 planar supercells in the simulation.

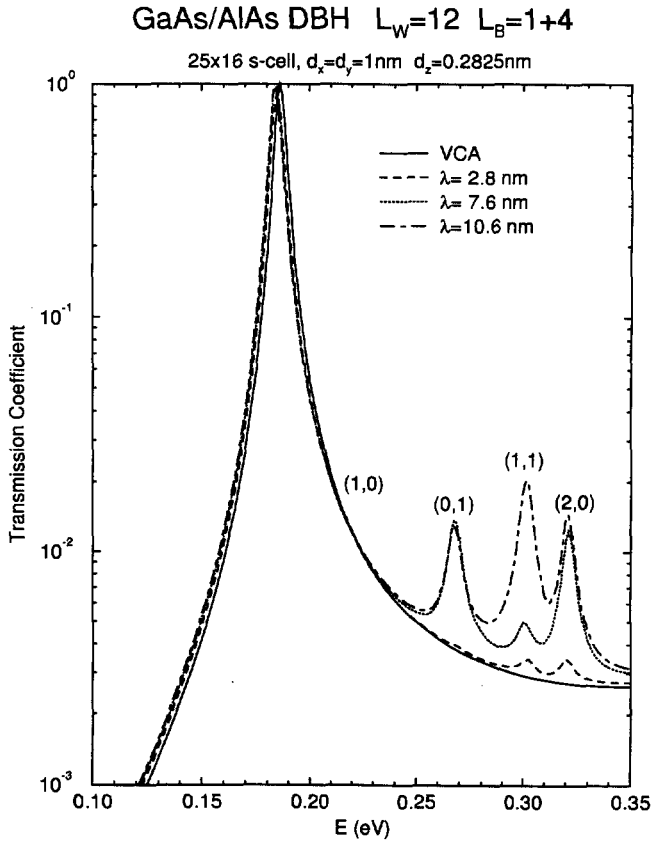

FIG. 3. Transmission coefficients for a set of GaAs/AlAs double barrier structures with $L_W=12$ GaAs wells and $L_B=4$ AlAs alloy barriers. For each GaAs–AlAs interface on the incident side, a 50% random coverage interface layer is placed between the pure GaAs layers and the pure AlAs layers. Interface layers with island sizes of $\lambda=28$, 76, and 106 Å are used. Also included for comparison is a structure where each of the two interface layers is replaced by a VCA $Al_{0.5}Ga_{0.5}As$ alloy layer. Discretization sizes of $d_x=d_y=10$ Å and $d_z=2.825$ Å are used with 25×16 planar supercells in the simulation.

indicates that the barriers with larger clusters are less confining. In barriers with GaAs clusters large enough to sustain localized states, additional peak structures are also induced in the transmission spectra.

Next we turn our attention to the effect of interface roughness on the transmission properties of double barrier structures. There are two types of interface roughness scattering effects: $\mathbf{k}_\parallel$ scattering and wave function localization. We first discuss $\mathbf{k}_\parallel$ scattering. Figure 3 shows the transmission coefficients for a set of GaAs/AlAs double barrier structures with $L_W=10$ GaAs wells and $L_B=4$ AlAs alloy barriers. The incident wave is chosen to have $\mathbf{k}_\parallel=0$. For each GaAs–AlAs interface on the left (incident) side of an AlAs barriers, a 50% random coverage interface layer is placed between the the pure GaAs layers and the pure AlAs layers. As before, the random configurations of the interface layers are generated with simulated annealing algorithm; island sizes, denoted by λ, of 28, 76, and 106 Å are used for this figure. Also included for comparison is a structure where each of the two interface layers is replaced by a VCA $Al_{0.5}Ga_{0.5}As$ alloy layer. Discretization sizes of $d_x=d_y=10$ Å and $d_z=2.825$ Å are used with 25×16 planar supercells in the simulation.

We note in Fig. 3 that for the island sizes under consideration, the $n=1$ resonance peaks for the structures with rough interfaces differ only slight from those for the structure with the smooth VCA interface layer; the peak positions are all within 5 meV. However, the spectra for the structures with rough interfaces show a series of satellite peaks not present in the VCA structure spectrum. The satellite peak strength increases with island size, but peak positions are the same for all three rough structures, even though the configurations of the interface layers differ substantially.

The satellite peaks are the result of $\mathbf{k}_\parallel$ scattering by the rough interfaces. From our earlier discussion we know that an incoming plane wave with zero parallel momentum can scatter into states with parallel momenta given by $\{\mathbf{g}_{lm}\}$, the parallel reciprocal lattice vectors of the planar supercell mini-Brillouin zone. Since for a plane-wave state with $\mathbf{k}_\parallel=\mathbf{g}_{lm}$, the double barrier band diagram is (to within a small decrease in the barrier height due to the fact that AlAs effective mass is larger than that of GaAs) just the $\mathbf{k}_\parallel=0$ band diagram shifted by

$$\Delta E_{lm}=E_{\mathrm{GaAs}}(\mathbf{k}=\mathbf{g}_{lm})-E_{\mathrm{GaAs}}(\mathbf{k}=0), \tag{4}$$

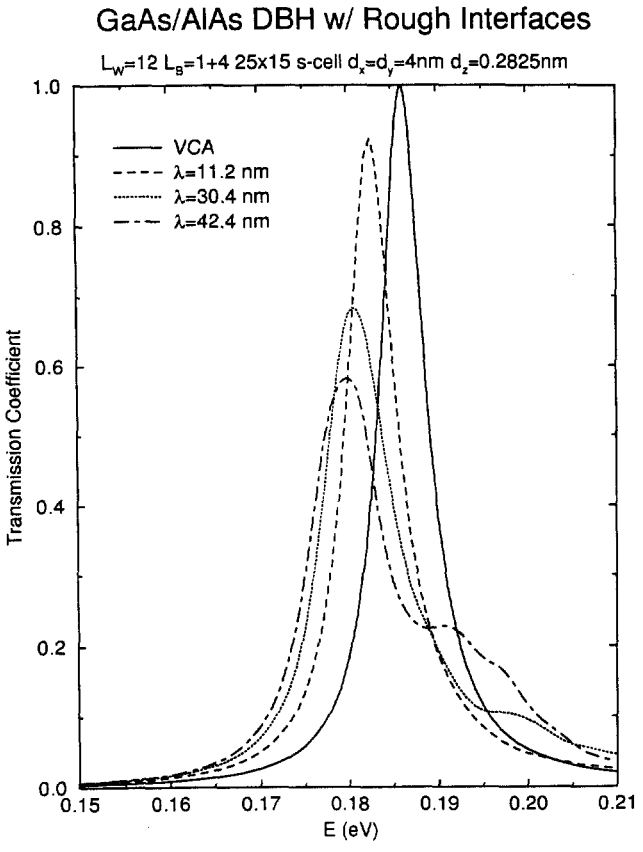

FIG. 4. Transmission coefficients for a set of GaAs/AlAs double barrier structures with $L_W=12$ GaAs wells and $L_B=4$ AlAs alloy barriers. For each GaAs–AlAs interface on the incident side, a 50% random coverage interface layer is placed between the the pure GaAs layers and the pure AlAs layers. Interface layers with island sizes of $\lambda=112$, 304, and 424 Å are used. Also included for comparison is a structure where each of the two interface layers is replaced by a VCA $Al_{0.5}Ga_{0.5}As$ alloy layer. Discretization sizes of $d_x=d_y=40$ Å and $d_z=2.825$ Å are used with 25×16 planar supercells in the simulation.

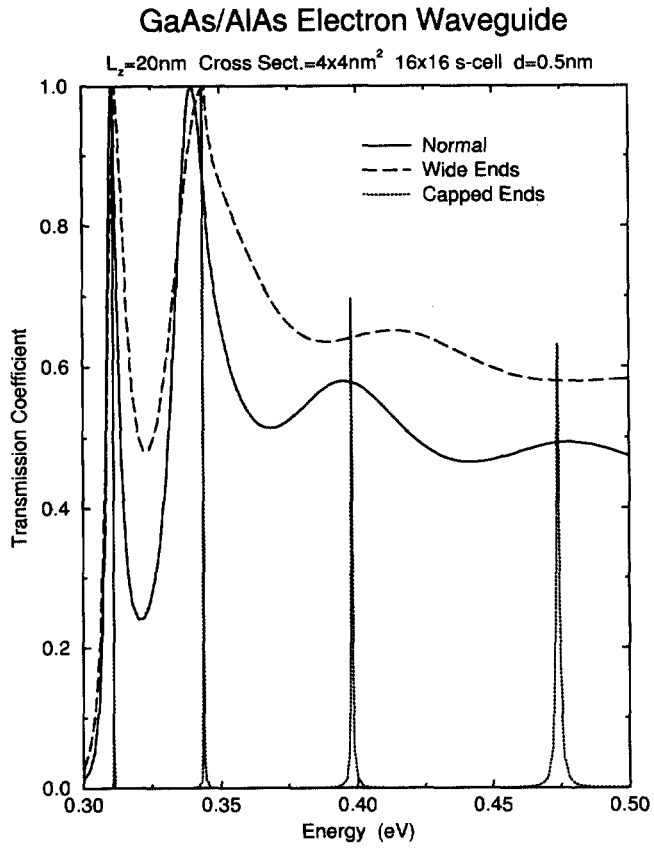

FIG. 5. The transmission coefficients for a GaAs/AlAs electron waveguide. The length of the waveguide is 200 Å, and the cross section is 40 Å$\times$40 Å. The size of the planar supercell is 80 Å$\times$80 Å. Also shown are the results for two similar structures, one with widened ends, and one with ends capped by added 15-Å-thick AlAs barriers. Discretization sizes of $d_x=d_y=d_z=5$ Å are used with 16×16 planar supercells in the simulation.

each scattered component should produce an $n=1$ resonance at ΔE_{lm} higher than the main $n=1$ resonance peak. Since $\mathbf{g}_{lm}$ is determined by the supercell size, the energy difference between the main peak and a satellite peak is therefore only a function of the supercell size, and is independent of the configuration within the supercell. Note that the density of satellite peaks increases with supercell size. In the limit of very large supercell sizes, the spacings between the satellite peaks would become smaller than the resonance peak width, and the satellite peaks would then coalesce. Note also that for small island sizes where the effect of interface scattering is minimal, we could model rough interface layers with smooth VCA alloy layers.

If the island sizes are sufficiently large, we could consider the quantum well as having wide-well ($L_W=13$, in this example) and narrow-well ($L_W=12$) regions. In that case, it is possible to have quantum well states whose wave functions are laterally localized in the wide-well regions. Since the wide-well regions are also the narrow-barrier regions, the transmission resonance associated with these localized states should be down shifted (due to the wider well), and broadened (due to the narrower barrier). To see this effect we need to go to larger island sizes. In Fig. 4 we again show transmission spectra around the $n=1$ resonance for a set of double barrier structures with different interface roughness configurations. These structures are identical to the ones in the previous example, except that the discretization sizes in the x and y directions have been increased to 40 Å so we could simulate larger islands.

Figure 4 shows clearly that the $n=1$ transmission resonance down shifts and broadens with increasing island size. For the structures with larger islands, shoulders near the main $n=1$ peak are seen. These are due to additional lateral modes localized in the wide well regions. Note also that the height of the $n=1$ peak decreases as island size increases; this is due to increased $\mathbf{k}_\parallel$ scattering.

As a final example we apply our method to a quantum wire electron waveguide. Using discretization sizes of $d_x=d_y=d_z=5$ Å and 16×16 planar supercells, we modeled a GaAs quantum wire structure 200 Å in length, and 40 Å$\times$40 Å in cross section, surrounded on the sides by AlAs walls; the electrodes are GaAs. To study the sensitivity of transport properties to the geometry of waveguide openings, we have modeled two similar structures. The first has slightly wider waveguide openings: at the two ends

of the waveguide, the cross section is widened to 60 Å×60 Å for the first 5 Å (lengthwise), and 50 Å×50 Å for the next 5 Å; the rest of the wire remains 40 Å×40 Å in cross section. The other structure is obtained by simply taking the original structure and capping the two ends with 15-Å-thick AlAs layers. Figure 5 shows the transmission spectra for the three structures described above. We see that the amplitude of the transmission coefficients and the resonance positions and widths vary considerably in these structures. This simple study demonstrates that the transmission properties are highly sensitive to the geometry of the waveguide openings.

IV. SUMMARY

We introduced the planar supercell method as a means to treat 3D quantum transport in mesoscopic tunnel structures. The flexibility of the method allows us to examine a variety of issues relevant to the operation of tunnel devices. Using this method, we have studied the transport properties of double barrier heterostructures with alloy barriers. We find that for alloy barriers with no clustering, the transport properties can be adequately modeled by the virtual crystal approximation. With clustering, the barriers become less confining with increasing cluster size. We also examined the effect of interface roughness on double barrier structures. We found that interface roughness introduces $\mathbf{k}_{\|}$ scattering which increases with island size. In the limit of large islands, lateral localization of the electron wave function also results in the down shifting and broadening of the resonance peaks. In addition, we found that the transport properties of quantum wire electron waveguides are highly sensitive to the geometry of waveguide openings.

ACKNOWLEDGMENTS

The authors would like to thank Eric Van de Velde, W. L. Johnson, and W. R. Frensley for helpful discussions. S. K. K. would like to thank the Office of Naval Research for graduate fellowship support during this research. This work was supported by the Office of Naval Research (ONR) under Grant No. N00014-89-J-1141.

[1]D. J. BenDaniel and C. B. Duke, Phys. Rev. **152**, 683 (1966).
[2]D. Z.-Y. Ting, E. T. Yu, and T. C. McGill, Phys. Rev. B **45**, 3583 (1992).
[3]R. W. Freund and N. M. Nachtigal, Numer. Math. **60**, 315 (1991).
[4]N. Metropolis, A. Rosenbluth, M. Rosenbluth, A. Teller, and E. Teller, J. Chem. Phys. **21**, 1087 (1953).